Pergamon

Int. J. Heat Mass Transfer. Vol. 40, No. 15, pp. 3703–3716, 1997

Printed in Great Britain
0017–9310/97 $17.00+0.00

PII: S0017–9310(96)00311–0

An experimental study of heat transfer in a simulated turbine blade cooling passage

W. D. MORRIS and S. W. CHANG

Department of Mechanical Engineering, University of Wales, Swansea, Singleton Park, Swansea SA2 8PP, U.K.

(*Received in final form* 9 *September* 1996)

Abstract—This paper describes an experimental investigation of heat transfer inside a simulated cooling channel for a gas turbine rotor blade. The channel is circular in cross-section and rotates about an axis which is orthogonal to its centre line. The study is aimed at the development of an experimental procedure and method of data processing which permits the determination of full axial and circumferential heat transfer data over the tube's inner surface. This is referred to as full field heat transfer data. In this respect a study of the combined effect of Coriolis and centripetal buoyancy forces on the forced convection mechanism inside the tube is the strategic aim. The experimental technique involved the determination of the inside surface temperature and heat flux distribution using a solution of the channel wall heat conduction equation. A series of wall temperature measurements on the leading and trailing edges of the channel, together with a prescribed electrically generated heat flux on the external surface, were used as boundary conditions with which to solve the channel wall heat conduction equation. The resulting internal heat flux distribution over the full inner surface was subsequently used to determine the local variation of heat transfer coefficient. The method was validated using data available in the technical literature and subsequently used to study the individual effects of Coriolis induced secondary flow and centripetal buoyancy using new data generated for the investigation. © 1997 Elsevier Science Ltd.

1. INTRODUCTION

Aircraft gas turbine engines require high cycle pressure ratios and high turbine entry temperatures to achieve high thrust to weight ratios with low specific fuel consumption. A suitably high gas temperature in the hot section of the engine (i.e. the combustor, turbine discs, and turbine stator/rotor blades) can only be achieved if some form of cooling is used for these components and high pressure air, bled from the compressor, is the customary coolant used in practice.

High pressure turbine rotor blades are particularly problematic. The airfoil sections must be able to sustain thermal and mechanical stresses, fatigue, creep and chemical deterioration experienced whilst maintaining an acceptable operating life.

The accurate prediction of the airfoil metal temperature distribution is the first step in the assessment of blade life. This requires the external heat transfer coefficient distribution over the airfoil surface and the internal coolant passage heat transfer coefficient distributions as boundary conditions for the solution of the conduction equation in the component domain. It has been demonstrated by Taylor [1] that an uncertainty of $\pm 10\%$ in the heat transfer coefficient distributions results in an uncertainty of $\pm 2\%$ in the metal temperature. This produces an uncertainty of $\pm 50\%$ on predicted blade life. The present paper is concerned with the determination of the internal cooling hole heat transfer coefficient distribution under different operating conditions.

Figure 1 illustrates the complexity of the coolant passages inside a rotor blade. A combination of film cooling, impingement cooling and convection cooling (utilising smooth-walled and artificially roughened channel surfaces) is used to satisfy the design requirements. Convection cooling channels are mainly orthogonal to the axis of the turbine with the coolant flowing in a root to tip or tip to root direction as shown in the figure. Prediction of the coolant flow field and the heat transfer coefficient distribution in these passages is extremely difficult due to the geometric features of the passages and also because the coolant rotates with the blade.

It has been well established that coolant flowing in these radially rotating channels is subjected to the combined effect of Coriolis force and centripetal buoyancy which severely alters the heat transfer obtained with forced convection ducted flow, see Morris and Ayhan [2], Wagner *et al.* [3] and Morris and Salemi [4], for smooth walled surfaces and Taslim *et al.* [5], Wagner *et al.* [6] and Morris and Salemi [7] for roughened surfaces.

With circular-sectioned channels, for example, Coriolis force creates a symmetrical cross stream secondary flow, see Fig. 2, with fluid from the central region moving towards the trailing edge and a return flow along the circumferential wall region towards the

NOMENCLATURE

A	constant coefficients
B_n	constant coefficients
Bu	fluid buoyancy parameter
C	axial location dependent coefficient
C_p	fluid constant pressure specific heat
D_1, D_2	constant coefficients
d	diameter of test section
E	constant coefficient
F	function of r
G	function of θ
k	fluid thermal conductivity
k_w	thermal conductivity of test section material
h	heat transfer coefficient
L	function of z
n	solution parameter
N	angular velocity of rotating frame
Nu	local Nusselt number
p	flow pressure
P	dimensionless pressure
Pr	fluid Prandtl number
q	heat flux
r	radial coordinate
$\mathbf{r}$	position vector
$\mathbf{R}$	dimensionless position vector
Re	Reynolds number
Ro	Rossby number
t	time
T	temperature
$\mathbf{v}$	velocity vector
$\mathbf{V}$	dimensionless velocity vector
w	mean axial flow velocity
Y_n	Bessel function solution
z	axial coordinate
Z	non-dimensional axial coordinate.

Greek symbols

β	fluid volume expansion coefficient
ρ	fluid density
μ	fluid dynamic viscosity
ν	fluid kinematic viscosity
ω	angular velocity vector
$\mathbf{\Omega}$	dimensionless angular velocity vector
η	dimensionless fluid temperature
Ψ	unknown function
Φ	unknown function
θ	angular coordinate.

Subscripts

i	inner tube surface
L	leading edge
m	measurement location
o	outer tube surface
0	zero rotational speed
R	reference condition
T	trailing edge
w	test section wall
z	axial location
θ	angular location.

leading edge. The net result of the pressure-driven flow in the root to tip direction and this secondary flow is a double helical flow pattern. This tends to improve heat transfer on the trailing edge of the channel relative to that on the leading edge. With a driven flow in the tip to root direction the direction of the secondary flow reverses.

With outward radial flow the axial velocity profile is asymmetrical with the maximum velocity location deflected towards the trailing edge as shown in Fig. 2. Centripetal buoyancy further modifies the flow field in a manner analogous to combined forced and gravitational free convection in vertical tubes where the radially outward orthogonal-mode rotation corresponds to a vertical tube with a downward flow.

The problem of predicting the flow and heat transfer inside this class of rotating tube is further complicated due to the fact that the rotation can alter the basic flow stability and turbulence structure, see Johnson [8], Johnson *et al.* [9], Koyama *et al.* [10, 11] and Rothe and Johnson [12].

The present paper presents the results of an experimental investigation which attempts to assess the effect of the combined Coriolis and buoyant interactions on the heat transfer mechanism over the entire surface of a smooth-walled circular tube which rotates in this orthogonal mode, thus simulating a rotating turbine airfoil cooling passage. The range of experimental variables over which tests have been conducted is extended beyond earlier published work by this research group and approaches the lower range of real engine conditions.

The full field heat transfer distribution over the entire tube surface is determined by solving the conduction equation in the tube wall. Thermocouple measurements of wall temperature at selected locations on the leading and trailing edge of the tube, together with a prescription of the external surface heat flux, give the required boundary conditions. Details of local heat transfer on the leading and trailing edges of the blade are treated initially and this is followed by an analysis of the full axial and circumferential heat transfer behaviour. This is referred to as full field data.

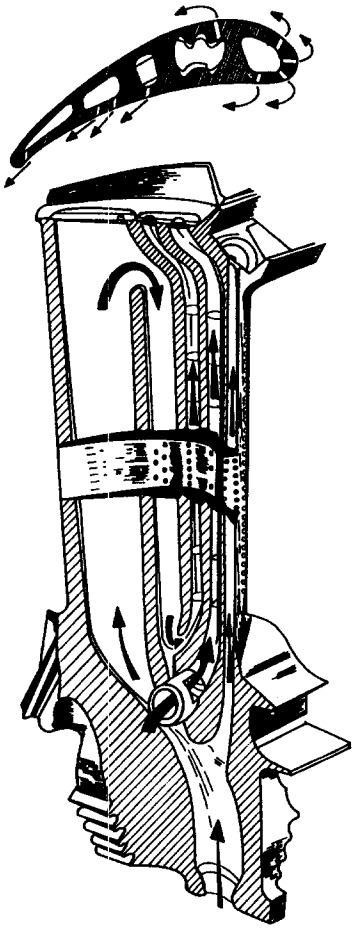

Fig. 1. Typical turbine rotor blade cooling channel network.

2. THE PHYSICAL PROBLEM

The flow field in the channel is controlled by the momentum conservation equations, but the inertial term has to be modified to account for Coriolis and centripetal accelerations because the flow is referred to a rotating reference frame. The influence of rotation may be explained by considering a laminar flow as follows. Consider a circular-sectioned tube rotating in the orthogonal mode as indicated in Fig. 2. The vector form of the momentum conservation equation is

$$\frac{D\mathbf{v}}{Dt}+2\boldsymbol{\omega}\wedge\mathbf{v}+\boldsymbol{\omega}\wedge\boldsymbol{\omega}\wedge\mathbf{r}=-\frac{1}{\rho}\nabla p+\mu\nabla^2\mathbf{v}. \quad (1)$$

All symbols are described in the Nomenclature.

The second two terms on the left-hand side of eqn (1) are the Coriolis and centripetal corrections, respectively. Implicit in eqn (1) is the fact that the fluid density and viscosity are considered to be invariant, at this stage. Examination of eqn (1), see Morris [13] for details, demonstrates that the Coriolis term, $2\,\boldsymbol{\omega}\wedge\mathbf{v}$, generates a cross stream secondary flow which causes the fluid to spiral in the streamwise direction. The centripetal term, $\boldsymbol{\omega}\wedge\boldsymbol{\omega}\wedge\mathbf{r}$, is conservative and only contributes to a hydrostatic effect in the flow. The net effect is that the Coriolis term is exclusively responsible for deviations in the flow field from the stationary duct situation.

With heated flow where the density is temperature dependent the centripetal term creates additional secondary effects via a buoyant interaction. This may be demonstrated as follows. Suppose the density of the fluid obeys the equation of state

$$\rho=\rho_R(1+\beta(T-T_R)) \quad (2)$$

Substitution of eqn (2) into eqn (1) and incorporating the Boussinesq approximation yields

$$\frac{D\mathbf{v}}{Dt}+2\boldsymbol{\omega}\wedge\mathbf{v}+(\boldsymbol{\omega}\wedge\boldsymbol{\omega}\wedge\mathbf{r})\beta(T-T_R)=-\frac{1}{\rho}\nabla p+\mu\nabla^2\mathbf{v}. \quad (3)$$

The so-called buoyancy force, $(\boldsymbol{\omega}\wedge\boldsymbol{\omega}\wedge\mathbf{r})\beta(T-T_R)$, now acts as an additional source term for modifying the stationary flow field.

In order to identify non-dimensional groups which describe this flow problem parametrically, the following variable transformations are made.

$$\mathbf{V}=\frac{\mathbf{v}}{w_m} \quad (4)$$

$$\boldsymbol{\Omega}=\frac{\boldsymbol{\omega}}{N} \quad (5)$$

$$\eta=\frac{(T-T_R)}{(T_w-T_R)} \quad (6)$$

$$P=\frac{p}{\rho_R w^2} \quad (7)$$

$$\mathbf{R}=\frac{\mathbf{r}}{d}. \quad (8)$$

Substitution of the transformed variables given by eqns (4)–(8) into eqn (3) yields, after some algebraic manipulations

$$\frac{D\mathbf{V}}{Dt}+\frac{(2\boldsymbol{\Omega}\wedge\mathbf{V})}{Ro}+Bu(\boldsymbol{\Omega}\wedge\boldsymbol{\Omega}\wedge\mathbf{R})=-\nabla P+\frac{\nabla^2\mathbf{V}}{Re} \quad (9)$$

where

$$Re=\frac{wd\rho_R}{\mu} \quad \text{(Reynolds number)} \quad (10)$$

$$Ro=\frac{w}{Nd} \quad \text{(Rossby number)} \quad (11)$$

$$Bu=\beta\frac{(T_w-T_R)}{Ro^2} \quad \text{(Buoyancy parameter).} \quad (12)$$

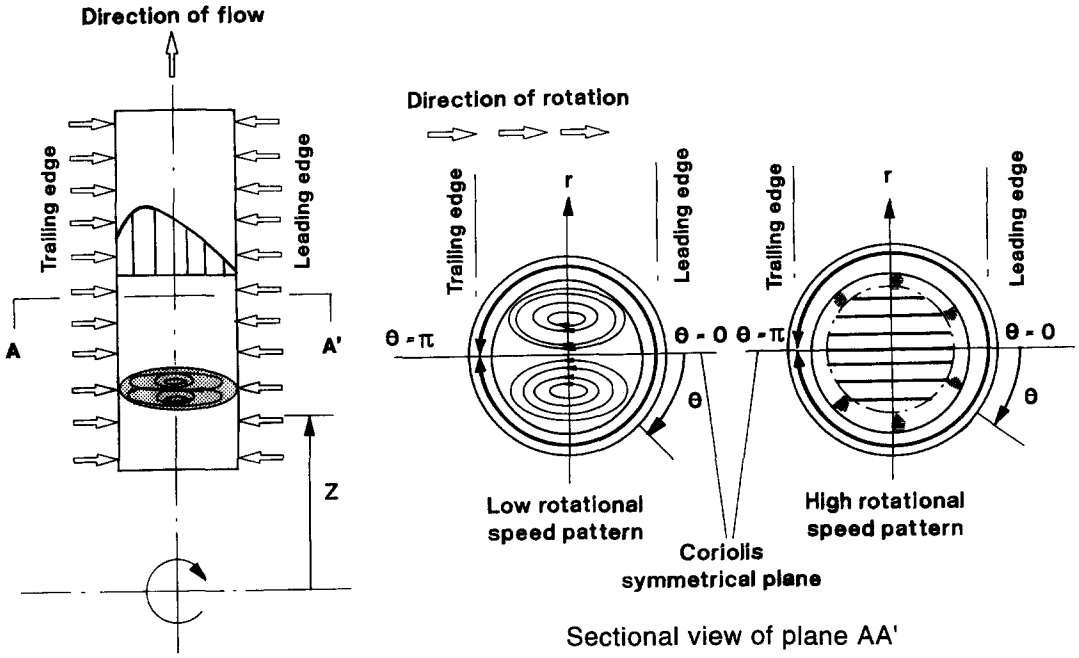

Fig. 2. Heat conduction mechanism taking place inside a rotating tube wall.

In addition to the momentum conservation equation, the energy conservation equation may be expressed in non-dimensional form as

$$\frac{D\eta}{Dt} = \frac{\nabla^2 \eta}{RePr} \tag{13}$$

where

$$Pr = \frac{\mu C_p}{k} \quad \text{(Prandtl number)}. \tag{14}$$

The detailed flow and temperature fields created in a particular situation will also depend on boundary conditions imposed. For example, the flow and thermal fields may develop together or in other cases the flow may be allowed to develop prior to the initiation of heating. Irrespective of boundary conditions, the non-dimensional groups identified by the above analysis will always be important. If local heat flux at any position on the surface of the duct is expressed via a local heat transfer coefficient, $h_{z,\theta}$, then we might expect a local Nusselt number to have the following structure for a specified set of boundary conditions.

$$N_{u_{\theta,z}} = \Psi(Re, Pr, Ro, Bu, Z, \theta) \tag{15}$$

where

$$N_{n_{\theta,z}} = \frac{h_{\theta,z} d}{k} \quad \text{(local Nusselt number)}. \tag{16}$$

This equation may be used as a guide to devise an experimental programme to study the effects of Coriolis and centripetal buoyancy forces.

3. APPARATUS

The rotating facility used for this investigation has been previously described, see Morris and Salemi [4]. Nevertheless, in the interest of completeness a brief description of this facility will be presented here together with a detailed description of the new test section which has been the subject of the present investigation.

The schematics of the facility are shown in Fig. 3. A hollow plenum chamber (1) contained the instrumented test section (2) and this was supported on a shaft (3). The shaft was mounted between bearings (4) and the assembly was driven by a DC motor (5) via a toothed belt drive (6). Pressurised, oil-free air was fed to the plenum chamber via a rotating seal (7). This seal incorporated two magnetically held face seals which were lubricated with an air/oil fog mixture. The cooling air entered the test section via the plenum and vented to atmosphere. To increase the range of inverse Rossby numbers over which tests could be undertaken, the exit end of the test section was fitted with nozzles (8) of varying diameter. In this way the plenum chamber pressure could be maintained above the critical choked flow condition permitting the air density increase to lower the mean axial velocity for a specified Reynolds number value.

A two channel power slip ring (9) permitted current from a transformer to be fed to a heater wrapped over the outer surface of the test section which is described below. Electrical power consumed by the heater was measured using an ammeter and voltmeter.

Thermocouple signals from the test section were

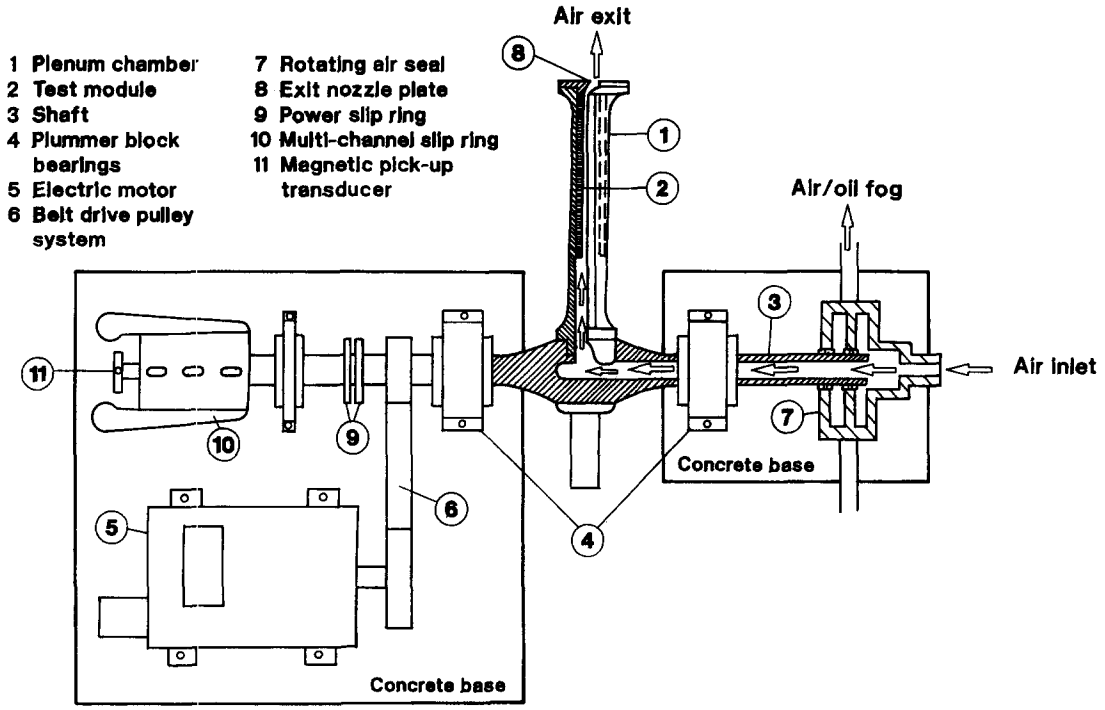

Fig. 3. Mechanical layout of rotating test facility.

taken from the rotor through a multi-channel slip ring (10) involving a series of shaft mounted silver rings rotating in contact with stationary silver/graphite brushes. The voltages from the thermocouples were fed to a Schlumberger Type S13535D data acquisition system and recorded on a Dell system 210 PC for subsequent data processing. Other required data were manually typed into the recording system as required.

The speed of the rotor was measured using a stationary magnetic encoder which detected the passage of iron inserts embedded into the periphery of a tufnol disc (11) which was attached to the instrumentation slip ring rotor shaft. The encoder was used in conjunction with a timer counter which gave a direct rotor speed read out.

The test section details are shown in Fig. 4. The heated tube (1) was made from stainless steel and had a bore diameter of 15 mm, a wall thickness of 1.5 mm and a nominal length of 253 mm. This tube was held between insulating bushes (2) and (3) to give a heated length of 225 mm between the faces of the supporting bushes. The bush/tube assembly was enclosed in an aluminium tube (4) fitted with external 'O' ring seals (5) at both ends.

A pair of twin start threads (see inset (6) in the figure), having the same pitch but differing depths, was machined onto the outer surface of the test tube to facilitate the installation of thermocouples and electrical heating wire. The deeper of the two grooves was used for embedding Type K thermocouples along the leading and trailing edges of the tube. The depth of this groove was arranged so that each thermocouple sensing junction was located 0.5 mm from the inner surface of the tube. Twelve thermocouples were attached to the leading and trailing edges as indicated in the figure. Thermocouples were also used to measure the temperature of the air upstream of the test section entry and located in the plenum chamber. Similarly, the temperature of the air leaving the test section was measured in the central region of bush (3). Nichrome resistance wire was used for the heating wire.

A cover plate (7) at exit from the test section incorporated a convergent nozzle which permitted control of the air density in the test section, as mentioned earlier. Grooves machined in this cover plate permitted access of the heater and thermocouple cables to their electrical circuitry. The space between the outer surface of the heated test section and the aluminium tube was back filled with thermal insulating foam to minimise external heat loss.

The test assembly was mounted in the air delivery plenum chamber (see item (1) in Fig. 3) and bolted in position with bolts passing through the matching holes on the cover plate (7) and a corresponding flange machined at the outer end of the plenum. The eccentricity of the entry station of the test section was 150 mm and this was set by means of an internal spacer bush fitted inside the plenum. Two diametrically opposed tubes (shown as (12) in Fig. 3) permitted all

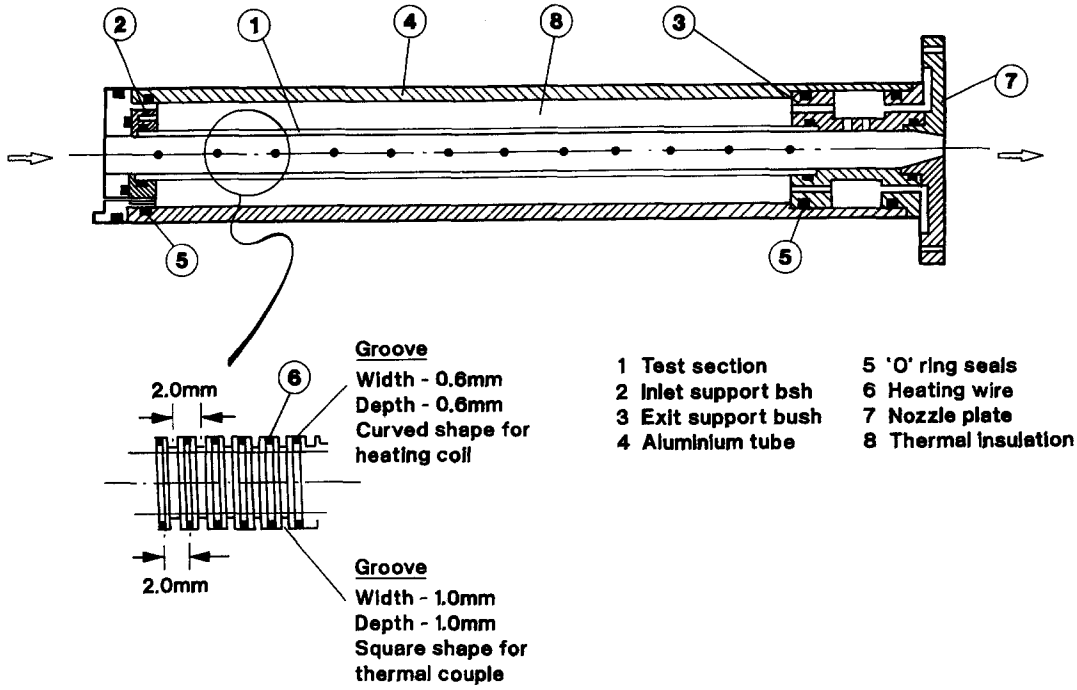

Fig. 4. Test section construction.

heater and thermocouple wires to be brought to the main rotor shaft and hence to the respective power and instrumentation slip rings via cables mounted in keyways machined on the main shaft. Silicon rubber was injected into these wire-carrying passages to inhibit chaffing movement and aid sealing.

4. METHOD OF DATA EVALUATION

Temperature measurements were taken along the leading and trailing edges of the tube via wall-embedded thermocouples at twelve downstream axial locations relative to the tube entry plane and the radial position of these thermocouples was specified. By independently varying the flow rate of coolant, the heating rate and the rotational speed it was possible to generate a series of experimental results over a range of Reynolds and Rossby numbers together with a systematic study of the buoyancy parameter at each Reynolds/Rossby pair. Using measurements of the leading and trailing edge wall temperatures, the cooling air inlet temperature and the external heat flux on the outer radius of the tube, it was possible to generate a full surface map of the heat transfer response indicated by the functional form of eqn (15).

The full field variation of heat transfer in the circumferential and axial directions was determined using a combination of insight, measured boundary conditions and an analytical solution of the heat conduction equation in the tube wall. It is accepted that the method is approximate at this stage but, even so, some interesting results have emerged. The method adopted is now described.

The steady state heat conduction within the wall material is given by,

$$\nabla^2 T_w = \frac{\partial^2 T_w}{\partial r^2} + \frac{1}{r}\frac{\partial T_w}{\partial r} + \frac{1}{r^2}\frac{\partial^2 T_w}{\partial \theta^2} + \frac{\partial^2 T_w}{\partial z^2} = 0. \tag{17}$$

During a rotating experiment there is a symmetry diameter across the leading and trailing edges due to the symmetry of the secondary flow generated. Thus there will be no conduction through the walls at the leading and trailing edges. Thus the solution of eqn (17) is subject to the boundary condition

$$\frac{\partial T_w}{\partial \theta} = 0 \quad \text{at } \theta = 0 \quad \text{and at } \theta = \pi. \tag{18}$$

Also, the heat flux at the outer radius, r_o, is specified as being uniform in the circumferential direction but variable in the axial direction due to external heat loss. The result is that this externally imposed heat flux, $q_o(z)$, is known and this gives an external surface boundary condition as

$$-k\frac{\partial T_w}{\partial r} = q_o(z) \quad \text{at } r = r_o. \tag{19}$$

Also we know the wall temperature at two measured locations corresponding to the leading and trailing

edge at a number of axial locations along the test section. Thus

$$T_w(r_m, 0, z_m) = T_L \quad \text{and} \quad T_w(r_m, \pi, z_m) = T_T. \tag{20}$$

Assume the wall temperature distribution may be expressed in separable variable form as

$$T_w = F(r)G(\theta)L(z) \tag{21}$$

where the three functions $F(r)$, $G(\theta)$ and $L(z)$ are only functions of one variable.

At any axial location, z_m,

$$\frac{\partial^2 T_w}{\partial z^2} = F(r)G(\theta)L(z)''. \tag{22}$$

Suppose we seek a solution to eqn (17) at a specified z-location, $L(z_m)$ and treat the unknown $L(z_m)$ and its second derivative, $L''(z_m)$, as known constants. We may hence re-write eqn (17), using eqns (10) and (21) as

$$\frac{r^2F''(r)+rF'(r)+Cr^2F(r)}{F(r)} = \frac{-G''(\theta)}{G(\theta)} = \pm n^2 \tag{23}$$

where n is some appropriate constant which satisfies the boundary conditions and

$$C = \frac{L''(z_m)}{L(z_m)}. \tag{24}$$

Solutions exist for the two cases $n^2 = 0$ and $+n^2$ and these result in a superimposed solution

$$T_w = \sum_{n=1}^{\infty} B_n Y_n(Cr)\cos n\theta + A\ln r + E \tag{25}$$

where B_n, A and E are constants and Y_n is the second type of Bessel function.

The two measured wall temperatures permit us to evaluate one term of the Bessel function and this is the accepted approximation in this first attempt at using this method. Thus

$$T = \left[\frac{D_1}{r} + D_2 r\right]\cos n\theta + A\ln r + E \tag{26}$$

where D_1 and D_2 are constants. The boundary conditions permit the specification of the four constants in eqn (26) as

$$D_1 = \frac{1}{2}\left[\frac{1}{r_m} + \frac{r_m}{r_0^2}\right]^{-1}(T_L - T_T) \tag{27}$$

$$D_2 = \frac{1}{2r_0^2}\left[\frac{1}{r_m} + \frac{r_m}{r_0^2}\right]^{-1}(T_L - T_T) \tag{28}$$

$$A = -\frac{q_0(z_m)r_0}{k} \tag{29}$$

$$E = -\frac{q_0(z_m)r_0}{k_w}\ln r_m + \frac{1}{2}(T_L + T_T). \tag{30}$$

Note that additional temperature measurements at other angular positions would permit higher order terms to be included in future. Here the approximation made is that the two temperature measurements permit a reasonable approximation to the determination of the full field temperature variation over the inner surface of the tube.

The circumferential heat flux variation, $q_i(\theta, z_m)$ at a specified z_m on the inner surface of the tube is calculated via

$$q_i(\theta, z_m) = -k_w\frac{\partial T_w}{\partial r} \quad \text{at } r = r_i. \tag{31}$$

Knowing the heat flux on the inner tube surface, via eqn (31) and the corresponding inner surface temperature distribution, via eqn (26), permits the circumferential distribution of heat transfer coefficient, $h(\theta, z)$ to be calculated at each axial location where measurements were made using the definition

$$h(\theta, z_m) = \frac{q_i}{T_w(r_i, \theta, z_m) - T_B(z_m)}. \tag{32}$$

In eqn (32) $T_B(z_m)$ is the fluid bulk temperature at location z_m. This is determined by an enthalpy balance on the fluid commencing at the inlet where the entry bulk temperature is known from direct measurement and using eqn (31) to specify the integrated heat flux between axial measuring stations. Finally a full field Nusselt number, $Nu(\theta, z_m)$, distribution could be generated from the evaluation of the above equations at each of the twelve axial measurement locations using eqn (16).

The circumferential variations of heat transfer coefficient which resulted were finally mapped using standard plotting software over the entire inner surface of the tube.

5. EXPERIMENTAL PROGRAMME

Initially a series of tests was undertaken at zero rotational speed to give a comparative reference base with which to assess the effect of rotation. Experiments were conducted over the Reynolds number range 10 000–35 000. For each Reynolds number, five different heat flux conditions were used. The heater powers were actually selected to give maximum wall temperatures of the test section of 50, 75, 100, 125 and 155°C, respectively. After completion of the zero rotational speed tests the programme was repeated at rotational speeds up to a maximum of 2000 rev min^{-1}.

For these tests the inverse Rossby number at the entry region to the test section was controlled to be constant at various rotational speeds by altering the flow rate. This meant that the influence of Reynolds number could be examined at a fixed inverse Rossby

number. The actual range of entry plane inverse Rossby numbers covered was 0–0.54.

Variation of the heater power permitted a systematic variation of the buoyancy effect at fixed inverse Rossby number/Reynolds number combinations. Because the Buoyancy parameter given by eqn (12) includes the Rossby number, the component $\beta(T_w - T_B)$ will be used as a convenient characterisation of buoyancy at the present stage of development of the method. Thus the difference in wall to bulk coolant temperature is used to describe buoyancy. The range of the $\beta(T_w - T_B)$ component of the Buoyancy parameter covered was 0.0–0.4.

The power dissipated by the heater is not entirely transferred to the coolant owing to external losses and conduction through the metallic walls. The external heat loss is dependent on the rotational speed and this was determined by means of heat loss experiments carried out prior to the main experimental programme. For these tests the coolant passage was filled with insulation and measurements of the wall temperature distributions taken over a range of heater settings at each of the rotational speeds used for the main test programme. In the steady operating state the heat generated by the heater was deemed to be lost to the environment via the difference in mean wall temperature and the ambient temperature. A plot of the heat loss against this temperature difference was found to be linear at all speeds. Consequently the local heat loss at any axial location during the main experiments could be assessed by assuming that the loss was directly proportional to the locally prevailing difference in wall to ambient temperature. For rotating experiments where the leading and trailing edges operate at different temperatures the average wall temperature was used to estimate the heat losses. In this way the axial variation of heat flux along the test section was prescribed being assumed to be girthwise uniform.

The wall temperature measurements on the leading and trailing edges of the tube and the axial heat flux were used to determine the circumferential variation of wall temperature at the inner bore of the tube using the results of Section 4. Also the actual circumferential heat flux transferred to the fluid at each measuring station was determined. The circumferential variation of the local Nusselt number could then be evaluated using the inner bore wall temperature, the heat flux and the fluid bulk temperature. A post processing graph plotting routine was used to plot the Nusselt number contours using the calculations from each axial measuring position.

6. RESULTS AND DISCUSSION

6.1. *Validation of the data processing method*

The approximate method for determining the full field heat transfer distribution described in Section 3 was validated using experimental data obtained within the research group by Al Merri [14]. This work involved a detailed measurement of the circumferential wall variation in a radially rotating tube at numerous axial locations using the same rotating facility as that of the present investigation. The data available were taken with a stainless steel test section of 10.0 mm bore, a wall thickness of 1.5 mm and a length of 130 mm. The eccentricity of the entry plane of the test section was 389 mm. For a range of rotational speeds, heat fluxes and Reynolds numbers the measured leading and trailing edge temperatures were used as input data for the prediction of the circumferential temperature variation using eqn (26). Figure 5 shows a selection of the comparisons between the detailed measurements and the current prediction method. The agreement is very agreeable and gave confidence in the use of the method with the new experiments presented in the present paper.

6.2. *Leading and trailing edge results*

For all non-rotating tests there was no systematic variation in the measured wall temperatures on the leading and trailing edges. This was consistent with the axisymmetric nature of the flow and forced convection heat transfer mechanism present. An examination of the local variation of Nusselt number demonstrated the well known approach to a terminal or fully developed Nusselt number which occurs as the flow and thermal boundary layers develop along the tube. At axial locations of about 10 diameters downstream of entry the Nusselt number was in good agreement with the Dittus and Boelter [15] correlation.

When the experiments were repeated with rotation it was immediately found that the temperatures measured on the leading and trailing edges were significantly different. Consistent with other studies of orthogonal-mode rotation, see Morris and Salemi [4], the leading edge was consistently at higher temperature than the trailing edge at any axial location. This was due to the Coriolis driven secondary flow, described earlier, causing relatively cool core region flow to move towards the trailing edge. Figure 6 illustrates the typical differences in wall temperature measured for a Reynolds number of 25 000, a rotational speed of 2000 rev min^{-1} and a variety of heat flux settings.

At zero rotational speed eqn (15) must reduce to the case of ducted flow forced convection. If $Nu_{0,z}$ represents the zero speed Nusselt number at any axial location, then we expected that for turbulent flow

$$N_{0,z} = Re^{0.8} Pr^{0.33} \phi(Z). \tag{33}$$

This means that eqn (15) will have the form

$$\frac{N_{0,Z}}{N_{0,z}} = 1 + \frac{\varphi(Re, Pr, Ro, Bu, Z, \theta)}{Re^{0.8} Pr^{0.33} \phi(Z)}. \tag{34}$$

Based on empirical data Morris *et al.* [16] have suggested that the overall effect of Reynolds number on the second term on the right-hand side of eqn (34) vanishes or, at least, is small. This means that

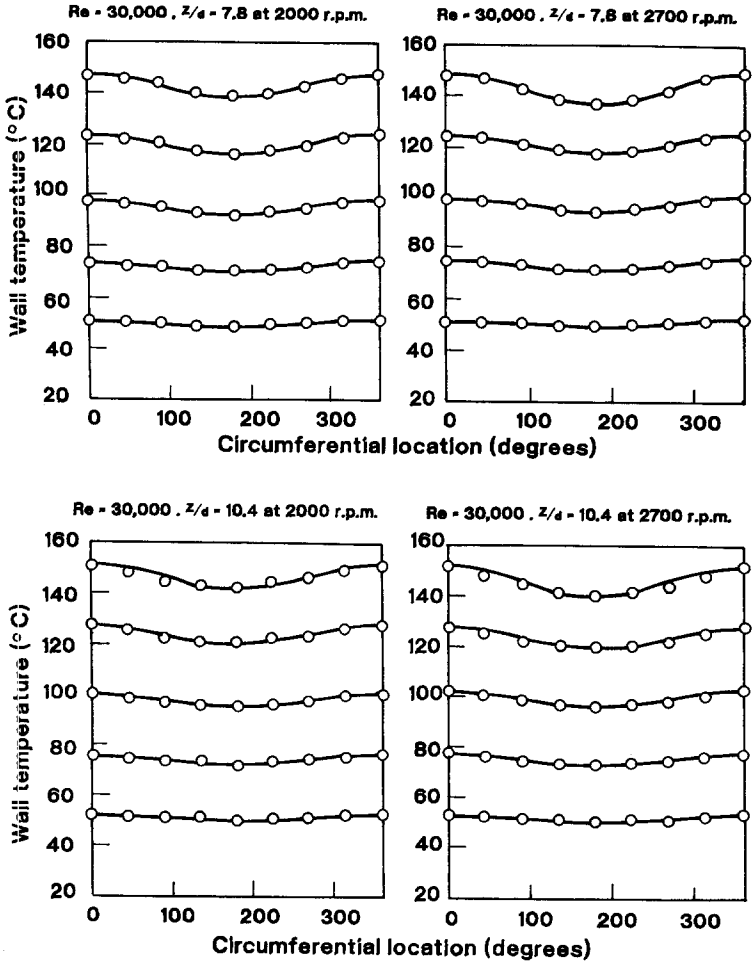

Fig. 5. Comparison of theoretical predictions with experimental results obtained from various rotational tests [14].

rotational data plotted in terms of the Nusselt number ratio $Nu_{\theta,Z}/Nu_{0,Z}$ would be independent of Reynolds number. In other words the effect of Reynolds number is fully accounted for via the 0.8 exponent appropriate to forced convection. This hypothesis was explored in the present study by conducting experiments with fixed values of the inverse Rossby number but made up with different combinations of flow and rotational speed. The results for the leading and trailing edges were used for the assessment of this hypothesis. A sample of the typical results obtained are given in Fig. 7. Here the ratio of the local Nusselt number on the leading and trailing edges scaled with the 0.8 power of the actual Reynolds number tested is plotted against axial location. Axial location is expressed in terms of the effective diameters downstream of entry. It should be noted that the experiments which produced the data points in Fig. 7 were controlled to approximately create the same average value of $\beta(T_w - T_B)$ so that the effect of centripetal buoyancy was being maintained constant during the series of tests. There is a strong tendency for data at fixed inverse Rossby number and variable Reynolds number to collapse onto a single line. This seems to substantiate the theory that Reynolds number effects may be taken into account through a normal stationary tube forced convection mechanism.

The influence of centripetal buoyancy was examined by conducting tests at fixed values of the Reynolds number and inverse Rossby number and varying the heat flux to give a variety of wall to fluid temperature differences. Thus forced convection and Coriolis secondary flow effects were maintained constant whilst the Buoyancy parameter was varied. Figure 8 illustrates the centripetal effects which were observed. As the heat flux is increased the local Nusselt number on the leading and trailing edges also increased significantly. In all cases the trailing edge is better cooled than the leading edge. Additionally it is noted that heat transfer on the leading edge can fall below the stationary tube level under certain operating conditions.

6.3. *Full surface heat transfer results*

Finally, the reverse engineering data processing method was used to study the individual effects of Coriolis secondary flow and centripetal buoyancy. A set of tests was undertaken with the average value of

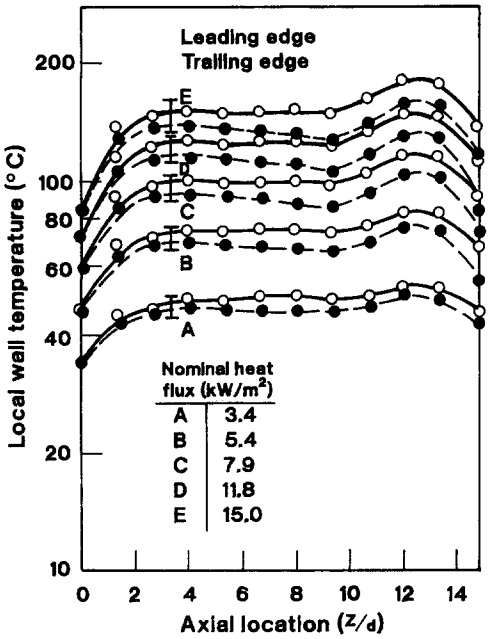

Fig. 6. Typical axial wall temperature distribution with system rotation: rotational speed = 2000 r.p.m.; Reynolds number = 25000; Inverse Rossby number = 0.166.

the term $\beta\,(T_w - T_B)$ maintained at approximately 0.3 in order to standardise the buoyancy effect. With this series of tests experiments were undertaken with inverse Rossby number values of 0.08, 0.15, 0.20, 0.40 and 0.47. The data process model was used to evaluate the circumferential variation in Nusselt number at each of the twelve axial measuring stations and the post processing interpolation software used to generate the full field variation. Figure 9 shows the derived Nusselt number variations which resulted.

The development of the three dimensional flow is clearly complex but certain features are worthy of note. As the inverse Rossby number increases the commencement of the circumferential variation of Nusselt number seems to occur nearer to the plane of entry. This indicates that the Coriolis induced secondary flow is making its presence felt almost immediately at the higher rotational speeds. For inverse Rossby numbers up to 0.4 there was some evidence that a fully developed Nusselt number distribution was forming at axial locations about 7–9 diameters downstream of entry. This is indicated by the tendency for the Nusselt number bands to be parallel in the circumferential direction. At higher values of inverse Rossby number the Nusselt number patterns are more complicated with a possibly stronger interaction with the exit region may be occurring.

Experiments were also conducted at a fixed value of the inverse Rossby number, namely 0.52, with five different external heat fluxes. In this way the effect of centripetal buoyancy was the subject of a systematic investigation. The heat flux levels gave average values of the $\beta(T_w - T_B)$ term of 0.07, 0.12, 0.17, 0.22 and 0.27. It was not possible to control the detailed variation of the wall to fluid temperature differences along the tube for all inverse Rossby number values tested and this is why an average value was used as a buoyancy variable.

Figure 10 shows the effect of buoyancy which resulted from the tests. The Nusselt number at all circumferential locations tended to increase with increases in the strength of buoyancy as already demonstrated above for the leading and trailing edges. At the relatively high value of inverse Rossby number in Fig. 10 there was no clear evidence of the formation of a traditional developed flow region. What is very evident from these systematic plots is the fact that buoyancy was a strong effect even with high levels of Coriolis cross flow. This is particularly important for the development of prediction methods for this effect must be included in the analysis. Indeed the Coriolis and buoyant forces are also likely to influence the turbulent flow structure itself.

7. CONCLUSIONS

The purpose of this paper has been to illustrate the use of a reverse engineered method for determining the full field heat transfer distribution in a radially rotating circular-sectioned tube, with application to the design of cooled gas turbine rotor blades. The method involves a solution of the heat conduction equation in the wall of the test section using measured temperatures and an externally prescribed heat flux as required boundary conditions. The salient points which have been demonstrated are as follows.

(1) The method has been validated against a set of experimental data which independently measured the circumferential variation in wall temperature in a radially rotating tube. The prediction of circumferential wall temperatures using the measured temperatures on the leading and trailing edges gave very good agreement with the subsequent girthwise predictions and the actual independently measured values.

(2) Experiments designed to test the validity of an empirical suggestion that the use of a forced convection Reynolds number effect, in the form of a 0.8 exponent of Reynolds number, has demonstrated that this is a strongly valid assumption. This will be a useful result for future attempts to derive empirical correlations for design purposes.

(3) The method has been shown to be able to discern systematic changes in the strength of the Coriolis driven secondary flow and also the centripetal buoyancy. The full interpretation of these interactive effects still requires additional experimental work to be undertaken, notably at near engine conditions. The method gives an additional useful tool for determining full field data from limited thermocouple spot measurements. The method may be refined if a num-

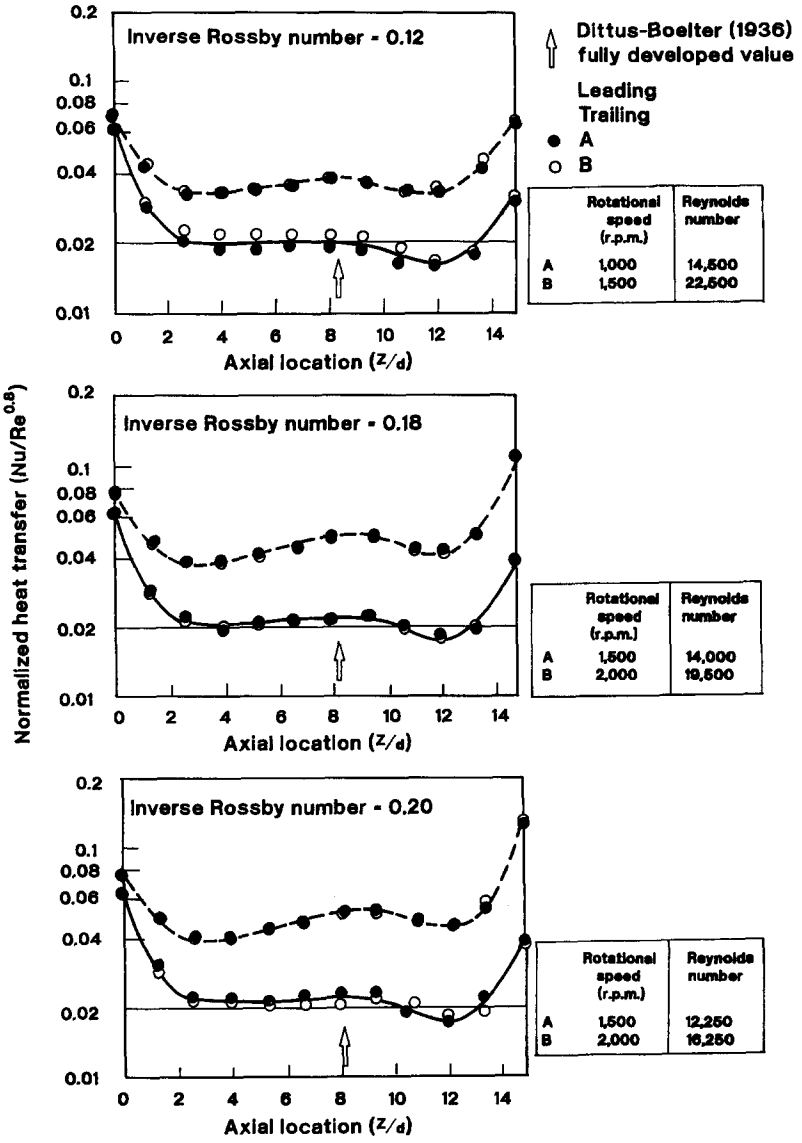

Fig. 7. Normalised axial heat transfer distribution at inverse Rossby number values of 0.12, 0.18 and 0.20.

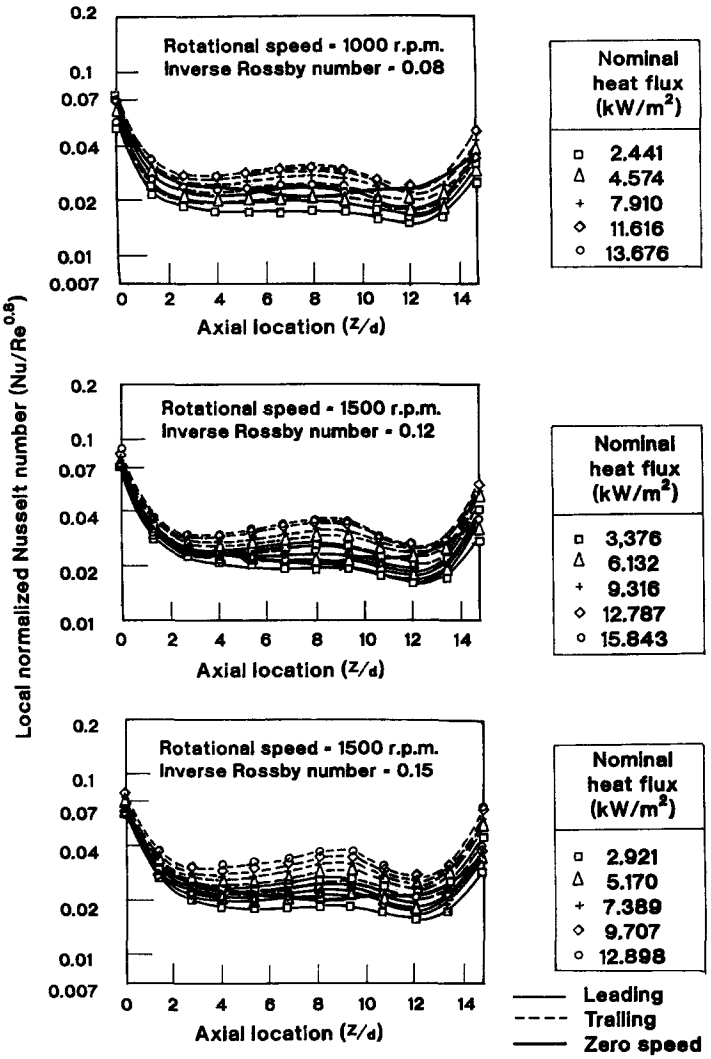

Fig. 8. Normalised axial heat transfer distribution with various centripetal buoyancy levels at fixed inverse Rossby numbers.

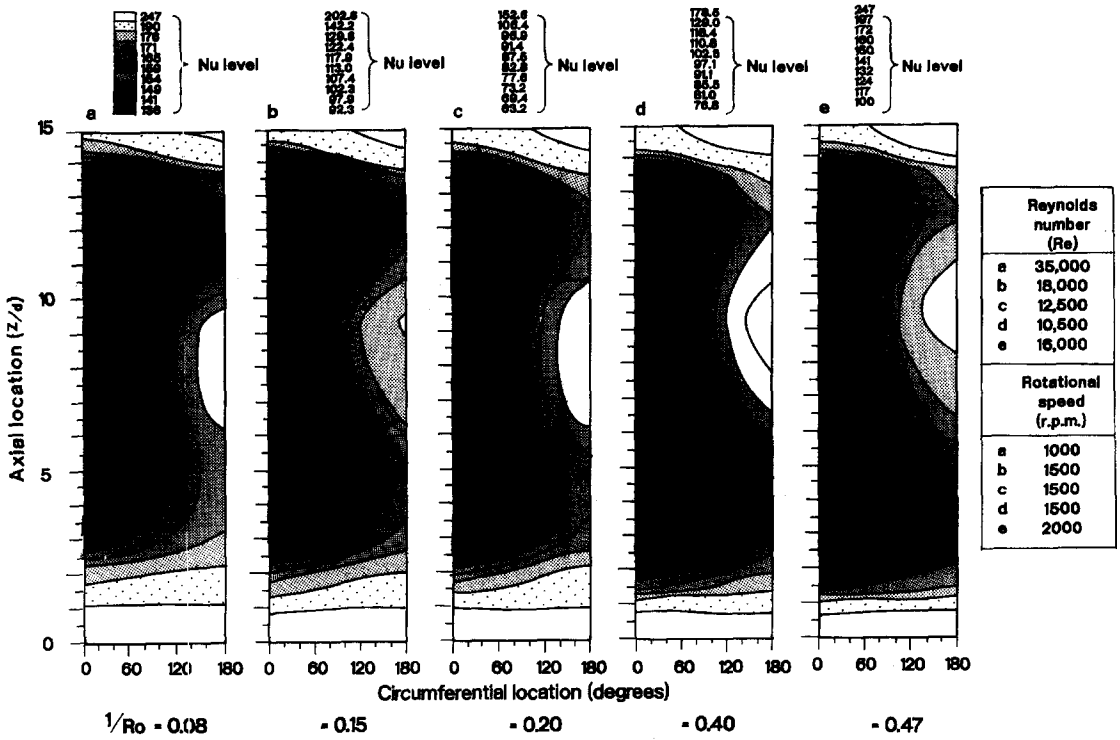

Fig. 9. Effects of Coriolis secondary flows on the heat transfer contours.

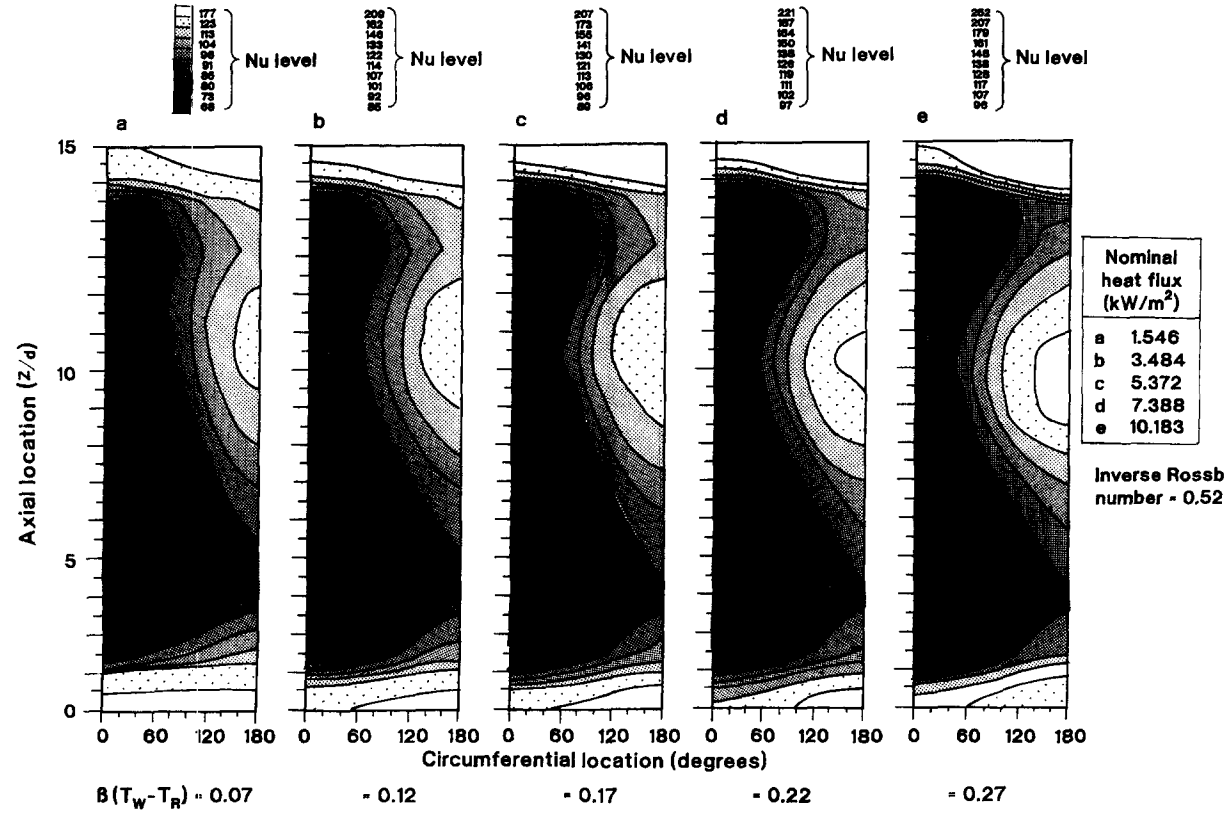

Fig. 10. Effects of buoyancy on the heat transfer contours.

ber of additional circumferential temperature measurements are permitted on the test facilities used.

(4) The method may be adopted for other non-axisymmetric ducted flow heat transfer problems.

Acknowledgements—The authors acknowledge the encouragement and support given by the Defence Research Agency and Rolls Royce, plc., for this ongoing research.

REFERENCES

1. Taylor, J. R., *Heat Transfer Phenomena in Gas Turbines*. ASME 80-GT-172, 1980.
2. Morris, W. D. and Ayhan, T., Observations on the influence of rotation in the coolant channels of gas turbine rotor blades. *Proceedings of the Institute of Mechanical Engineers*, 1979, **193**(21), 988.
3. Wagner, J. H., Johnson, B. V. and Hajek, T. J., Heat transfer in rotating passages with smooth wall and radial outward flow. *ASME Gas Turbine and Aeroengine Congress and Exposition*, Toronto, Canada, 1989.
4. Morris, W. D. and Salemi, R., An attempt to uncouple the effect of Coriolis and buoyancy forces on heat transfer in smooth circular tubes which rotate in the orthogonal mode. *Transactions of ASME, Journal of Turbomachinery*, 1991, **114,** 858.
5. Taslim, M. E., Rahman, A. and Spring, S. D., An experimental investigation of heat transfer coefficients in a spanwise rotating channel with two opposite rib-roughened walls. *ASME Gas Turbine and Aeroengine Congress and Exposition*, Toronto, Canada, 1989.
6. Wagner, J. H., Johnson, B. V., Graziani, R. A. and Yeh, F. C., Heat transfer in rotating serpentine passages with trips normal to the flow. *ASME Gas Turbine and Aeroengine Congress and Exposition*, Orlando, FL, 1991.
7. Morris, W. D. and Salemi, R., The effect of orthogonal mode rotation on forced convection in a circular-sectioned tube fitted with full circumferential transverse ribs. *AGARD Conference Proceedings* 527, *Heat Transfer and Cooling in Gas Turbines*, Anatalia, Turkey, 1992.
8. Jonson, J. P. *AGARD Conference on Turbulent Shear Flows*, AGARD Current Paper no. 93, 1971.
9. Jonson, J. P., Halleen, R. M. and Lezius, D. K., Effects of spanwise rotation on the structure of two-dimensional fully developed turbulent channel flow. *Four. Fluid Mechanics*, 1972, **56,** 553.
10. Koyama, H., Masuda, S. and Watanabe, I., Stabilizing and destabilizing effects of Coriolis forces on two-dimensional laminar and turbulent boundary layers. *ASME, Journal of Fluids Engineering*, 1979, **101,** 117.
11. Koyama, H., Ariga, I., Masuda, S. and Watanabe, I., Turbulence structure and three-dimensionality of a rotating two-dimensional turbulent boundary layer. *2nd Symposium on Turbulent Shear Flow*, Imperial College, London, 1979.
12. Rothe, P. H. and Johnson, J. P., Free shear layer behaviour in rotating systems. *ASME, Journal of Fluids Engineering*, 1979, **101,** 117.
13. Morris, W. D., *Heat Transfer in Rotating Coolant Channels*. Research Studies Press, Wiley, New York, ISBN 0 471 10121 4, 1981.
14. Al-Merri, A. A., Heat transfer in smooth tubes rotating in the orthogonal mode. Ph.D. thesis, University of Wales, Swansea, 1990.
15. Dittus, F. W. and Boelter, L. M. K., Californian Pubs, *Engineering*, 1936, **2,** 443.
16. Morris, W. D., Harasgama, S. P. and Salami, Measurements of turbulent heat transfer on the leading and trailing surfaces of a square duct rotating in the orthogonal-mode. *ASME Gas Turbine and Aeroengine Congress and Exposition*, Amsterdam, Netherlands, 1988.